Pyrene-based covalent triazine framework towards high-performance sensing and photocatalysis applications

Guang Cheng[1†], Kewei Wang[2†], Shengyao Wang[4†], Liping Guo[1], Zijian Wang[3], Jiaxing Jiang[3], Bien Tan[1] and Shangbin Jin[1*]

ABSTRACT Porous organic polymers (POPs) are an emerging class of porous materials, having many promising applications in a variety of areas. Among them, covalent triazine frameworks (CTFs) featuring conjugated and porous structures can be well applied in optoelectronics. To achieve high optoelectronic performance, usually the design and synthesis of CTFs based on appropriate building blocks is critical. Here we report the synthesis of two fluorescent CTFs based on typical fluorescent building blocks, in which CTF-Py constructed from a pyrene (Py) building block was reported for the first time, showing prospective applications in the sensing of nitroaromatics with high sensitivity, and photocatalytic water splitting and carbon dioxide reduction with high performance in comparison with other porous organic materials.

Keywords: covalent triazine frameworks, pyrene, fluorescent, water splitting, carbon dioxide reduction

INTRODUCTION

Porous organic polymers (POPs) which are an emerging class of porous materials derived from organic building blocks have received wide scientific and technical attention [1,2]. Various types of structural and functional POPs, such as covalent organic frameworks (COFs) [3–9], conjugated microporous polymers (CMPs) [10–12], hyper-crosslinked polymers (HCPs) [13], polymers of intrinsic microporosity (PIMs) [14,15], and covalent triazine frameworks (CTFs) [16–20], are developed. They have been widely explored in many applications including gas adsorption, catalysis, sensing and optoelectronics [1,2,20–26]. On the other hand, thin-layered morphology has also extensively attracted enormous attention because of the advantages given by the ultrathin thickness of the materials [27–29]. For example, the thin layers can shorten the migration distances of the excited charges for reducing the recombination probability and the endowed large surface areas would provide abundant sites that are beneficial to chemical sensing and catalysis [30]. The COFs with layered morphologies have been reported as photoluminescent materials and shown good sensing properties [31]. Some CMPs and HCPs with layered morphologies were also reported for photocatalysis [32,33].

CTFs are porous polymers with conjugated structure, high chemical stability and high nitrogen content. The ionothermal synthetic method of CTFs exploited high temperature that went along with partial carbonization, making the CTFs not adaptable for optical applications [16]. After that, a CF_3SO_3H-catalyzed approach was invented to synthesize CTFs, by which fluorescent CTFs could be acquired and their bandgap structures could be retained [20]. The CTFs obtained by this method have exhibited potential optical applications in the sensing of nitroaromatic compounds or photocatalytic water splitting [25]. Recently, a solution synthesis strategy of thin-layered CTFs that were grown in the interface of superacid and solvent was demonstrated for a promising application in field-effect transistor [34]. Although many progresses have been achieved using the above methods,

---

[1] Key Laboratory of Material Chemistry for Energy Conversion and Storage, Ministry of Education-School of Chemistry and Chemical Engineering, Huazhong University of Science and Technology (HUST), Wuhan 430074, China
[2] Department of Chemistry and Chemical Engineering, Shanxi Datong University, Datong 037009, China
[3] School of Materials Science and Engineering, Shaanxi Normal University, Xi'an 710062, China
[4] College of Science, Huazhong Agricultural University, Wuhan 430074, China
[†] These authors contributed equally to this work.
[*] Corresponding author (email: jinsb@hust.edu.cn)

there are still some disadvantages, such as the partial carbonization or the limitation of the building blocks in the synthesis and applications.

To further overcome these limitations, we have recently shown an effective low-temperature polycondensation reaction to synthesize CTFs at mild conditions, which allows various building blocks to be used [35]. By this route, the CTFs could be designed from versatile building blocks and show high potentials in photocatalysis applications. In order to achieve excellent performance in the applications, it is important to select or design appropriate building blocks in the structures of the polymers. Therefore, many structures have been adopted in the synthesis of CTFs. However, some other meaningful building blocks remain rarely explored in the construction of photofunctional CTFs. For example, fluorescent units like pyrene (Py) and tetraphenylethene (TPE) have been widely explored in the synthesis of porous polymers, such as COFs or CMPs, which can be applied in sensing or other optoelectronic applications [36–39]. TPE block has been reported to synthesize CTF by using the superacid catalysis method [25,26], but the synthesis of TPE-based CTFs using the polycondensation reaction remains undeveloped. Moreover, Py unit has not yet been used in the synthesis of CTFs, although it has already been reported in the synthesis of other useful porous materials for various promising applications [36,37]. Thanks to the highly conjugated structure and fluorescent properties, the synthesis of CTFs based on these building blocks may promisingly result in porous materials with excellent optoelectronic applications.

Along this line, here we report the synthesis of two new CTFs constructed from Py and TPE units by the new polycondensation reaction for the first time. In particular, the pyrene unit was originally used for the synthesis of CTFs, which showed good fluorescence properties and thin-layered morphologies [35]. The as-prepared CTFs have found encouraging performance in chemical sensor for the detection of explosive chemicals with high sensitivity. The CTFs also have great potentials in photocatalysis applications, which exhibit good performance in hydrogen evolution and carbon dioxide reduction thanks to the porous conjugated system and wide visible light absorption. These performances surpass many other reported porous materials.

EXPERIMENTAL SECTION

Materials
Methanol, ethanol, 1,4-dioxane, tetrahydrofuran, *N,N*-di-

methyl formamide (DMF), dimethyl sulfoxide (DMSO), HCl, and anhydrous potassium carbonate were purchased from the National Medicines Corporation Ltd. of China. 1,3,6,8-Tetrabromopyrene and cesium carbonate were purchased from Energy Chemical. 4-Formylphenylboronic acid was purchased from TCI. Tetrakis(triphenylphosphine)palladium was bought from Sigma-Aldrich. Tetra (*p*-formylphenyl) pyrene (TFPP) and tetra (*p*-formylbiphenyl)-ethylene (TFBPE) were synthesized according to literature methods [40,41]. Terephthalamidine dihydrochiloride was synthesized according to our previous report [35].

General procedure for the preparation of CTFs
Synthesis of CTF-Py. A round-bottom flask was charged with TFPP (0.309 g, 0.5 mmol), terephthalamidine dihydrochiloride (0.470 g, 2 mmol), cesium carbonate (1.304 g, 4 mmol) and 10 mL of DMSO. The mixture was heated at 60°C for 12 h, 80°C for another 12 h, then 100°C, and finally continuously heated at 120°C for three days to obtain an orange solid. The crude product was washed with dilute HCl (3×10 mL) to remove the residual cesium carbonate and washed with DMF (3×10 mL) to remove the unreacted monomer or the oligomer, then washed with ethanol (3×10 mL) and deionized water (3×10 mL). The solid was dried by freeze-drying for two days to afford an orange powder (0.61 g, 96% yield).

Synthesis of CTF-TPE. The procedure was similar to the above except that TFBPE (0.222 g, 0.5 mmol) was used instead of TFPP. The final solid was dried by freeze-drying for two days to afford an orange powder (0.46 g, 90% yield).

Instruments and methods
The morphologies were measured by using field emission scanning electron microscopy (FE-SEM, FEI Sirion 200 field emission scanning electron microscope). The CTF powders were put on copper studs by using adhesive graphite tape and then coated with carbon before the observation. Nitrogen adsorption/desorption measurements of the CTFs were carried out volumetrically by using a Micromeritics ASAP 2020 M surface area and porosity analyzer (Micromeritics, USA). The surface areas were obtained from the nitrogen adsorption data by Brunauer-Emmett-Teller (BET) or Langmuir equation. Pore size distributions were derived from the isotherms using the nonlocal density functional theory (NLDFT) model based on a slit pore geometry. Thermogravimetric analyses (TGA) of CTFs were carried out using a heating rate of 10°C min^{-1} under a nitrogen atmosphere, with a

PerkinElmer Diamond TG/DTA instrument. Fourier transform infrared (FT-IR) spectra of CTFs were obtained in the wavenumber range of 4000–400 cm^{-1} using a Bruker VERTEX 70 FT-IR Spectrometer (Bruker, Germany). UV-visible spectra in the solid-state were characterized by a Shimadzu UV-3600 spectrophotometer. Powder X-ray diffraction (XRD) pattern of CTFs were characterized by a Siemens D5005 diffractometer. Time-resolved fluorescence decay profiles were obtained by Edinburgh instruments FLS-980. Atomic force microscopy (AFM) images of CTFs were observed on a scanning probe microscopy SPM-9700 instrument (Shimadzu Japan). In a typical process for the AFM sample preparation, 2 mg of CTF powders were added into 10-mL centrifuge tubes. Then, 8 mL of ethanol or isopropanol (IPA) was added into the above tubes as dispersion solvents, and the tubes were sonicated for 10 h, and left undisturbed overnight. Finally, a drop of the dispersed CTF solution was dripped to the mica sheet followed by drying for 15 min under a hot lamp.

Photochemical and electrochemical measurements

The fluorescence quenching experiments were investigated at room temperature by adding explosive compounds with variable concentrations to the CTF dispersion. For a general procedure, 1 mg of CTFs was dispersed in 40 mL of DMF with ultrasonication for 30 min, and then different analysts (2,4,6-trinitrophenol (TNP), dinitrotoluene (DNT), nitrobenzene (NB), *p*-nitrotoluene (*p*-NT), from 0 to 20 ppm) were added to the CTFs.

The electrochemical characterizations were conducted in a typical three-electrode cell system by using a CHI60E electrochemical workstation (Chenhua, Shanghai). The working electrodes were prepared on indium-tin-oxide (ITO), which were thoroughly cleaned up by sonication in ethanol for 30 min. The CTF powders (5 mg) were mixed with 0.5 mL of ethanol and 1 mL of 1‰ Nafion by sonication to get a slurry, which was then spread onto the ITO surface. The uncoated parts of the electrode was separated with epoxy resin, and the exposed area of the electrode was estimated to be 1 cm^2. The Pt plate and Ag/AgCl electrode (3 mol L^{-1} KCl) were used and worked as the counter electrode and reference electrode, respectively. 0.2 mol L^{-1} Na$_2$SO$_4$ aqueous solution was used as the electrolyte. The time-correlated photocurrent response measurements were conducted under visible light generated by a 300 W xenon lamp (Beijing, Perfect light). The electrochemical impedance spectroscopy (EIS) experiments were carried out on the IMP-A.C. Impedance

workstation. Mott-Schottky experiments were taken on an IMPE-Impedance Potential workstation, and the potential ranged from −0.3 to 0.8 V. Photocatalytic water-splitting experiments were measured under visible light (>420 nm) with a 300-W Xe lamp (Perfectlight, PLS-SXE300). The CTF samples (50 mg) were dispersed in 100 mL of aqueous solution with 10 vol% triethanolamine (TEOA). Pt (3 wt%) was introduced as a co-catalyst by *in-situ* photodeposition using H$_2$PtCl$_6$ precursor. The temperature of the solution was maintained at room temperature by using a circulating cooling water system. The hydrogen evolution rates were evaluated by SHIMADZU gas chromatography (GC-2014C) equipped with a thermal conductive detector (TCD) and a 5A molecular sieve column. The CO$_2$ photoreduction experiments were performed in a gas-closed system equipped with a gas-circulated pump (Makuhari Rikagaku Garasu inc., Japan). The catalyst (10 mg), 45 mL of solution (acetonitrile/water=7:2), 5 mL of TEOA and the Co (II) bipyridine complexes were mixed in a Pyrex glass reaction cell which was connected to the CO$_2$ reduction system. After evacuation of the catalysis system (no O$_2$ or N$_2$ could be detected by gas chromatography), pure CO$_2$ gas (~80 kPa) was injected into the airtight system. After the adsorption equilibrium, a 300 W xenon lamp (~100 mW cm^{-2}) with a UV-cut filter (L42) was used as the light source (λ>420 nm). The produced H$_2$ and CO were analyzed by gas chromatographs (GC-2030-BID, Shimadzu Corp., Japan).

RESULTS AND DISCUSSION

Structural characterization of CTFs

The CTFs are denoted as CTF-Py and CTF-TPE, respectively (Fig. 1a). The formation of the triazine linkage and network structures were clearly proved by the FT-IR spectra as well as solid-state carbon CP-MAS NMR spectra (Fig. 1b and c). The strong peaks at 1523 and 1355 cm^{-1} in the FT-IR spectra indicated the formation of a triazine ring in the frameworks.

In the solid-state ^{13}C-CP-MAS NMR, the chemical shift at 165.4 ppm was assignable to the carbon signal from triazine rings, confirming the formation of triazine units. The thermogravimetric analysis showed that the CTF-Py had higher thermal stability than CTF-TPE, which was up to 450°C (Fig. S1, Supplementary information). When the sample was tested in the oxygen atmosphere at 800°C, there was little residue after the high-temperature treatment. Fig. S2 shows the contents of the residues are only about 4.2 and 1.9 wt% for CTF-TPE and CTF-Py, re-
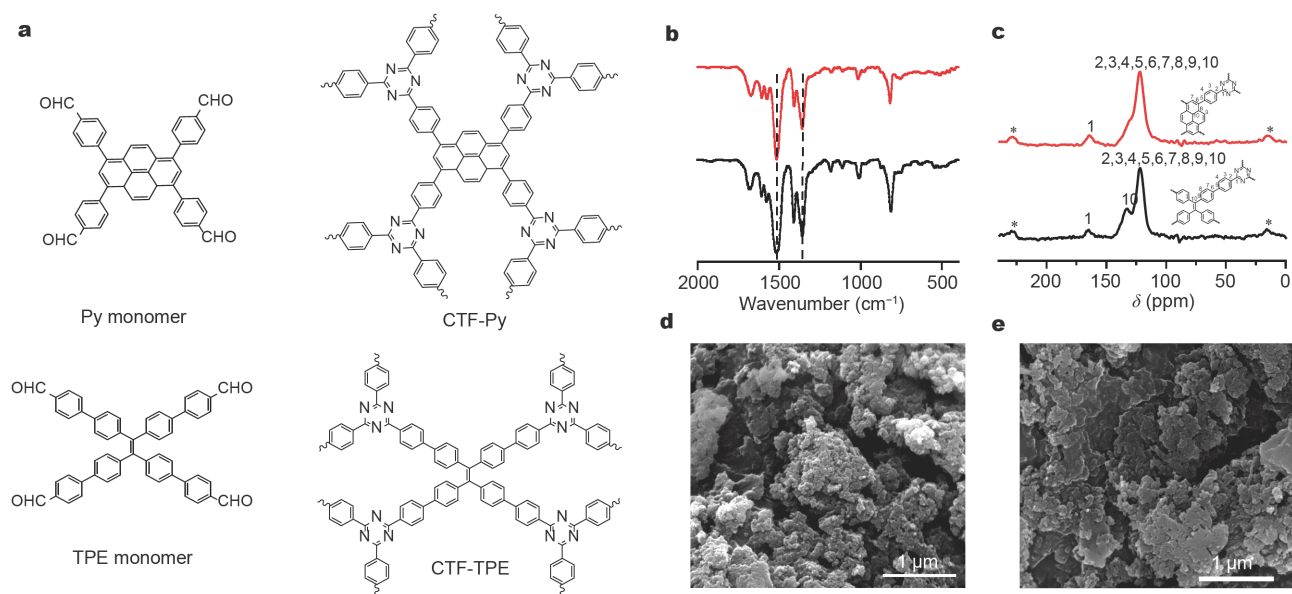
Figure 1 (a) Representative structures of CTF-Py and CTF-TPE and their monomers. (b) FT-IR spectra and (c) CP-MAS-^{13}C-NMR spectra of CTF-TPE (black) and CTF-Py (red); FE-SEM images of (d) CTF-TPE and (e) CTF-Py.

spectively, which may be attributed to the residual carbon. Figs S3 and S4 describe the X-ray photoelectron spectroscopy (XPS) results for the CTFs. Signals corresponding to the elements of C, N, O, Cl and Cs were observed in the spectrum survey. High-resolution XPS profiles were recorded in the N 1s, Cl 2p, Cs 3d regions. The N 1s spectrum can be deconvoluted into two peaks which are ascribed to pyridinic nitrogen (399.2 eV for CTF-TPE, 399.0 eV for CTF-Py) and pyrrolic nitrogen (400.5 eV for CTF-TPE, 399.9 eV for CTF-Py). Meanwhile, Fig. S4c and d show the Cl 2p spectrum which can be unambiguously assigned to chloride according to the binding energy derived from the wash reagent [42]. No signal corresponding to Cs 3d was detected for both CTFs. Combining the TGA in air and the XPS quantification analysis (Table S1), we may conclude that there was almost no catalyst residual. The elemental analysis of CTFs nearly matched the calculated values (Table S2) derived from the hypothetical fully condensed polymers, with only some small deviations which was normally observed in other microporous materials due to the adsorption capability for water and gases [10].

The morphologies of the resulting CTFs were observed by FE-SEM. CTF-TPE and CTF-Py exhibited particulate-like (Fig. 1d and e) and plate-like morphologies, respectively. The layered morphology was observed by transmission electron microscope (TEM) and high-resolution TEM images (Fig. S5), in which the layer edges were obviously seen from Fig. S5c and d. AFM images further

confirmed the sheet-like morphologies of CTFs which may be formed by π-π stacking of CTF layers. As shown in Figs S6 and S7, CTF-TPE possesses an average layer thickness of around 2 nm and CTF-Py has an average layer thickness of 4–5 nm. Powder XRD measurements only display broad reflection peaks at around 26° which can be attributed to the π-π stacking, revealing the resulting CTFs are disordered (Fig. S8). In principle, the CTFs synthesized in this work should form a three-dimensional (3D) network structures, and they usually do not form 2D layered structures. Unexpectedly, the layered morphologies of CTFs are probably due to the defective 3D network and π-π stacking structures.

The nitrogen sorption of the CTFs display the characteristic type IV isotherm curves (Fig. 2a). The BET surface areas of CTF-TPE and CTF-Py were calculated to be 673 and 508 m^2 g^{-1}, respectively. The pore size distributions showed that both CTFs were mainly microporous polymers, with some portions of mesoporous and macroporous structures (Fig. 2b).

Fluorescence properties and sensing application
Fluorescence spectra shows that CTF-Py and CTF-TPE exhibit yellow fluorescence in the solid-state (Fig. S9). The excitation peak of CTF-Py appears at 469 nm, and its emission peak is found at 544 nm in the solid-state (Fig. S9a). And the excitation peak of CTF-TPE is observed at 468 nm and its emission peak emerges at 552 nm in the solid-state (Fig. S9b). When the CTFs were
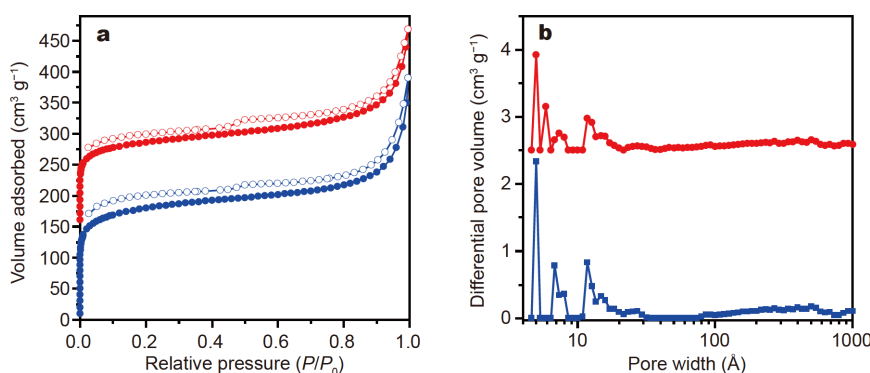
Figure 2 (a) Nitrogen adsorption-desorption isotherms of CTF-Py (red) and CTF-TPE (blue) at 77.3 K, (for clarity, the isotherms of CTF-Py was shifted vertically by 150 cm^3 g^{-1}) and (b) pore size distribution calculated using DFT methods (slit pore models, differential pore volumes of CTF-HUSTs).

dispersed in DMF, CTF-Py showed an obvious blue shift, in which the excitation peak was found at 396 nm and the emission peak appeared at 497 nm (Fig. 3a). However, the CTF-TPE exhibited a much weaker fluorescence in DMF (Fig. S10). The excitation peak of CTF-TPE dispersion was blue-shifted to 436 nm, and the emission peak blue-shifted to 535 nm [36,37,43,44].

After revealing the emission properties of the CTFs, we further investigated their application for sensing some explosive compounds. A series of nitroaromatics with gradient concentrations, i.e., TNP, DNT, NB, *p*-NT, were added to the CTF dispersion in DMF to monitor the emissive response (Fig. 3b and Figs S11, S12). The fluorescence is largely quenched when the concentration of TNP was gradually increased in the suspension (Fig. 3b). The fluorescence intensity of CTF-Py is reduced by 81%, while CTF-TPE also shows a 67% quenching degree when the concentration of TNP is up to 20 ppm (Fig. S13). Therefore, CTF-Py and CTF-TPE are more sensitive to TNP as compared with other nitroaromatics.

The quenching performance of CTF-Py is comparable to other CTFs or COFs in literature reports [25,44,45]. For example, the quenching efficiency of CTF-Py for TNP is higher than that of PCTF-8 which maximally quenches 71% of the fluorescence emission intensity [25]. It is also higher than some COFs system, such as Py-Azine COF quenching 69% and 3D-Py-COF quenching 75% of the fluorescence emission intensity [45,46]. The Stern-Volmer curve quenching constant (K_{SV-TNP}) of CTF-Py towards quenching of TNP was estimated to be 5.98×10^4 (mol L^{-1})$^{-1}$ (Fig. S14), which is also comparable to other reported porous materials [25,47,48].

To further understand the quenching mechanism, the fluorescence lifetimes before and after adding TNP were measured. As shown in Fig. S15, the fluorescence lifetime is independent of quenching substance, which suggests a likely static quenching mechanism. As well known, the TNP is a strong protonic acid due to the three nitro groups on the benzene ring. Hence, the CTFs act as bases to be sensitive to the phenolic hydroxyl groups of TNP
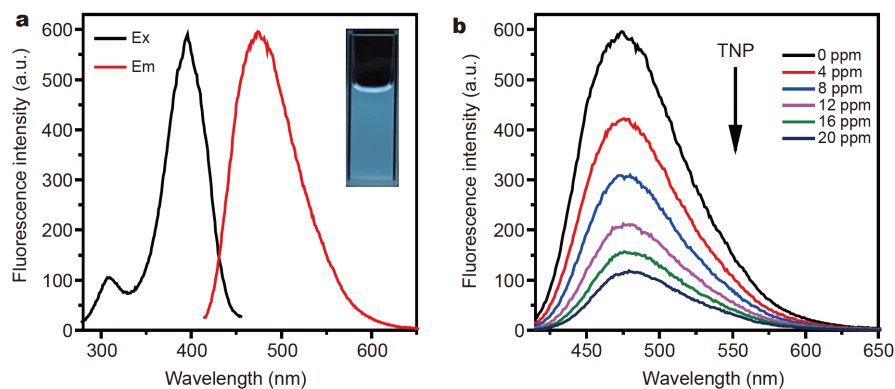
Figure 3 (a) Fluorescence spectra of CTF-Py dispersed in DMF; (b) fluorescence spectra of CTF-Py dispersed in DMF after introduction of different concentrations of TNP.

molecules and TNP can intensely interact with the triazine ring of CTFs [25,49]. Although it is far from the real applications, these results demonstrate the present CTFs are promising candidates for sensing applications.

Photocatalysis applications

The UV-vis absorption spectra show the CTFs can absorb visible light up to 700 nm in the solid-state (Fig. 4a). From the Kubelka-Munk-transformed reflectance spectra (Fig. S16), the optical band gap of CTF-Py was estimated to be 2.05 eV and that of CTF-TPE was 2.11 eV. Furthermore, the conduction bands and valence bands (CB and VB) were calculated based on the electrochemical Mott-Schottky plots (see Fig. S16c and d). The positive slope indicated typical n-type semiconductor behavior for both CTFs. Another meaningful parameter derived from the Mott-Schottky plots is the flat-band potential, which is roughly estimated to be −1.21 and −1.32 V versus Ag/AgCl for CTF-TPE and CTF-Py, respectively. It is noted that the potential of the CB of CTF-Py is higher than that of CTF-TPE, which may provide a larger dynamic driving force for photocatalysis. Fig. 4b shows the time-correlated photocurrent curves, and the periodic currents indicate

the CTFs are responsive to light irradiation, resulting from the charge separation and transfer. As shown in Fig. 4c, the energy level diagrams of the resulting CTFs are described. The conduction bands of the two CTFs are more negative than the H^+/H_2 redox potentials, implying the prospective application in the photocatalytic hydrogen evolution. EIS Nyquist plots (Fig. S17) studied the charge transfer rate in the dark. It is expected to have the semicircular Nyquist plots for both CTF-TPE and CTF-Py, but a slightly shrunken diameter appears on CTF-Py, indicating the faster charge migration. As shown in Fig. S18, fluorescent decays belong to a double-exponential profile. The fluorescence lifetimes of CTF-TPE are τ_1=0.72 ns (99.04%) and τ_2=3.97 ns (0.96%), and the average lifetime is estimated to be 0.75 ns. However, the fluorescence lifetimes of CTF-Py are τ_1=1.05 ns (48.59%) and τ_2=4.64 ns (51.41%) and the average lifetime is 2.90 ns which is longer than the CTF-TPE. The longer fluorescence lifetime means the photogenerated electrons would boost the surface reactions which can promote the photocatalytic activity [50,51].

To show the potentials of the CTFs in the photocatalytic water splitting, the photocatalytic hydrogen
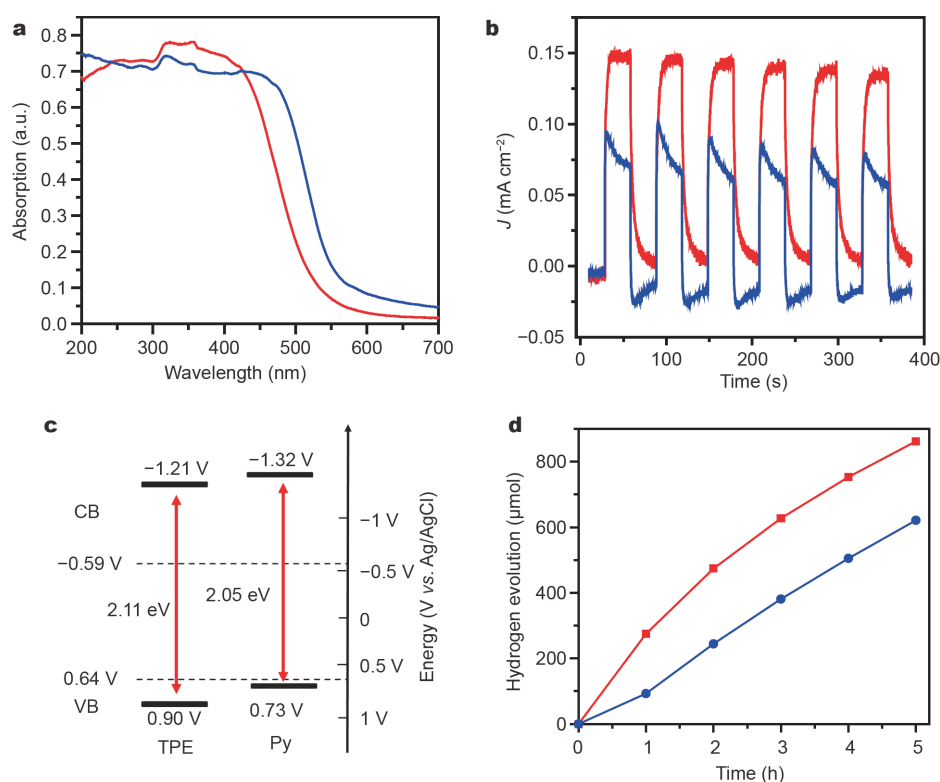

Figure 4 (a) UV-vis spectra of CTF-Py (blue) and CTF-TPE (red); (b) time-correlated photocurrents of CTF-TPE and CTF-Py under visible light irradiation; (c) band structure alignments of CTF-TPE and CTF-Py; (d) time courses of photocatalytic hydrogen evolution of CTF-Py (blue) and CTF-TPE (red) under visible light irradiation (>420 nm).

evolution was measured in a mixture of 100 mL TEOA/H_2O ($V{:}V$ = 1:10), in which TEOA worked as the sacrificial electron donor. In addition, 3 wt% Pt was loaded on the surface of the materials by an *in-situ* photoreduction method which played the role of co-catalyst. We can observe that an obvious photoluminescent quenching and a shortening of the photoluminescent lifetime after loading Pt nanoparticles (Figs S19 and S20). It indicated the Schottky junction was formed after loading nanoparticles, resulting in the suppression of the photoexcited charge recombination in CTF-Py and generating a new electron-transfer channel [52]. As revealed in Fig. 4d, both CTFs display high photocatalytic hydrogen evolution performance. CTF-TPE has a hydrogen evolution rate of 125 μmol h^{-1} (2500 μmol h^{-1} g^{-1}), and CTF-Py possesses a higher rate of 154 μmol h^{-1} (3080 μmol h^{-1} g^{-1}). The photocatalytic performance of CTF-Py is higher than that of CTF-2 and comparable to other reported CTFs, such as PCTF-8 which showed a photocatalytic activity of 118.5 μmol h^{-1} g^{-1}, and other porous organic polymers (Table S3) [8,25,35,53]. The activity of CTF-Py slightly decreased after several cycles (Fig. S21).

It is noted that longer fluorescence lifetime of CTF-Py than CTF-TPE is better for photocatalysis, while shorter lifetime of Pt@CTF-Py is in favour of photocatalysis. The contradictory trend of the fluorescence lifetime is because the fluorescence is generated *via* two different processes. In the photocatalysis process, the electrons in CTFs are at first excited and moved to the excited state and then would return to its ground state by fluorescence emission if there is no Pt nanoparticles. After loading with the co-catalyst Pt, the excited electrons are captured and the fluorescence is obviously quenched because of the elec-

tron transfer from CTF to Pt nanoparticles. The initial step is actually a charge recombination process, which is generally against photocatalysis if there is no further co-catalyst (Pt nanoparticles). However, if the non-platinized CTFs have longer fluorescence lifetime, the CTF may generate more excited electrons with longer existing time to migrate to Pt nanoparticles and thus it would benefit the photocatalysis process. Therefore, the contradictory trend of the fluorescence lifetime is because of the different mechanisms and both of them are beneficial to the photocatalysis in this work. It is also found that the photocurrent is inconsistent with the photocatalytic performance. This is probably due to the photocatalyisis is mainly influenced by other factors, such as the more negative lowest unoccupied molecular orbital (LUMO) energy levels and the broader light absorption of CTF-Py as compared with CTF-TPE.

Furthermore, photocatalytic carbon dioxide reduction was investigated. The photocatalytic performance of 10 mg CTFs under visible light (with 420 nm cut-off filter) was measured using 45 mL of CH_3CN/H_2O solvent, 5 mL of TEOA as the sacrificial agent and 5 μmol of $Co(bpy)_3Cl_2$ as a co-catalyst under ~80 kPa of pure CO_2 gas over 8 h (Fig. 5a). In the photocatalytic products, both CO and H_2 are found, but the CO is the major product with a high selectivity. CTF-Py has a high CO evolution rate of 13.73 μmol h^{-1} (1373 μmol h^{-1} g^{-1}) and a higher CO selectivity of 95.4% as compared with CTF-TPE (rate of 3.26 μmol h^{-1}, selectivity of 85.5%). The recycling experiment also shows the CTF-Py has an excellent recyclability over 5 times (Fig. 5b). These values are also comparable to other porous materials (Table S4) [54,55]. The isotope labelling experiment proves the resulting CO product is originated from CO_2 (Figs S22–S24). These
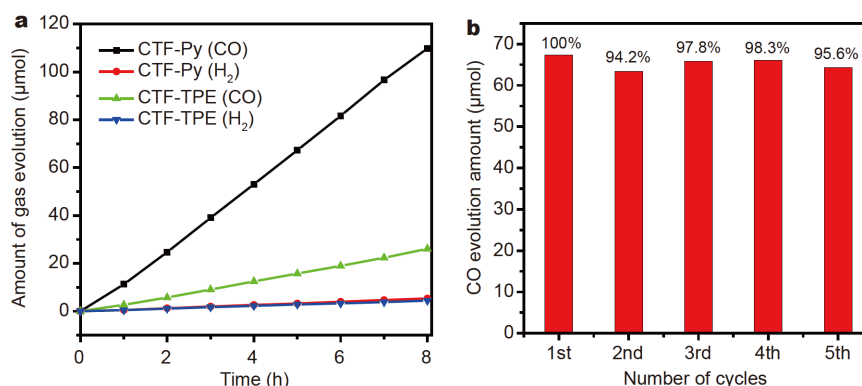
Figure 5 (a) Time courses of the CO evolution for CTFs over 8 h under visible light (using 420 nm cut-off filter) in 35 mL CH_3CN, 10 mL H_2O, 5 mL TEOA, and 5 μmol $Co(bpy)_3Cl_2$ as a co-catalyst over 10 mg CTFs under ~80 kPa of pure CO_2 gas; (b) recyclability of CTF-Py in the photocatalytic CO_2 reduction for 5 h over five cycles.

results further demonstrate the present CTFs are promising candidates for photocatalysis applications.

CONCLUSIONS

In summary, we report a new approach to construct fluorescent CTFs based on the polycondensation method. Among them, the resulting layered CTF-Py displays good fluorescence properties, which is potential for sensing application. The broad visible light absorption and layered nanostructures further enable photocatalytic applications in hydrogen evolution and carbon dioxide reduction with high performances. In particular, the photocatalytic carbon dioxide reduction performance is comparable to many other porous materials. Therefore, this work further demonstrates that the polycondensation approach is a useful tool to construct various porous materials for applications.

1 Wu D, Xu F, Sun B, *et al.* Design and preparation of porous polymers. Chem Rev, 2012, 112: 3959–4015

2 Das S, Heasman P, Ben T, *et al.* Porous organic materials: Strategic design and structure-function correlation. Chem Rev, 2017, 117: 1515–1563

3 Cote AP. Porous, crystalline, covalent organic frameworks. Science, 2005, 310: 1166–1170

4 Wan S, Guo J, Kim J, *et al.* A belt-shaped, blue luminescent, and semiconducting covalent organic framework. Angew Chem Int Ed, 2008, 47: 8826–8830

5 Spitler EL, Dichtel WR. Lewis acid-catalysed formation of two-dimensional phthalocyanine covalent organic frameworks. Nat Chem, 2010, 2: 672–677

6 Ding SY, Gao J, Wang Q, *et al.* Construction of covalent organic framework for catalysis: Pd/COF-LZU1 in Suzuki-Miyaura coupling reaction. J Am Chem Soc, 2011, 133: 19816–19822

7 Kandambeth S, Mallick A, Lukose B, *et al.* Construction of crystalline 2D covalent organic frameworks with remarkable chemical (acid/base) stability *via* a combined reversible and irreversible route. J Am Chem Soc, 2012, 134: 19524–19527

8 Stegbauer L, Schwinghammer K, Lotsch BV. A hydrazone-based covalent organic framework for photocatalytic hydrogen production. Chem Sci, 2014, 5: 2789–2793

9 Pang ZF, Xu SQ, Zhou TY, *et al.* Construction of covalent organic frameworks bearing three different kinds of pores through the heterostructural mixed linker strategy. J Am Chem Soc, 2016, 138: 4710–4713

10 Jiang JX, Su F, Trewin A, *et al.* Conjugated microporous poly (aryleneethynylene) networks. Angew Chem Int Ed, 2007, 46: 8574–8578

11 Cooper AI. Conjugated microporous polymers. Adv Mater, 2009, 21: 1291–1295

12 Chen L, Honsho Y, Seki S, *et al.* Light-harvesting conjugated microporous polymers: Rapid and highly efficient flow of light energy with a porous polyphenylene framework as antenna. J Am Chem Soc, 2010, 132: 6742–6748

13 Tan L, Tan B. Hypercrosslinked porous polymer materials: Design, synthesis, and applications. Chem Soc Rev, 2017, 46: 3322–3356

14 Budd PM, Ghanem BS, Makhseed S, *et al.* Polymers of intrinsic microporosity (PIMs): Robust, solution-processable, organic nanoporous materials. Chem Commun, 2004, 230

15 McKeown NB, Budd PM. Polymers of intrinsic microporosity (PIMs): Organic materials for membrane separations, heterogeneous catalysis and hydrogen storage. Chem Soc Rev, 2006, 35: 675–683

16 Kuhn P, Antonietti M, Thomas A. Porous, covalent triazine-based frameworks prepared by ionothermal synthesis. Angew Chem Int Ed, 2008, 47: 3450–3453

17 Kuhn P, Forget A, Su D, *et al.* From microporous regular frameworks to mesoporous materials with ultrahigh surface area: Dynamic reorganization of porous polymer networks. J Am Chem Soc, 2008, 130: 13333–13337

18 Bojdys MJ, Jeromenok J, Thomas A, *et al.* Rational extension of the family of layered, covalent, triazine-based frameworks with regular porosity. Adv Mater, 2010, 22: 2202–2205

19 Zhu X, Tian C, Mahurin SM, *et al.* A superacid-catalyzed synthesis of porous membranes based on triazine frameworks for CO_2 separation. J Am Chem Soc, 2012, 134: 10478–10484

20 Ren S, Bojdys MJ, Dawson R, *et al.* Porous, fluorescent, covalent triazine-based frameworks *via* room-temperature and microwave-assisted synthesis. Adv Mater, 2012, 24: 2357–2361

21 Xu Y, Jin S, Xu H, *et al.* Conjugated microporous polymers: Design, synthesis and application. Chem Soc Rev, 2013, 42: 8012–8031

22 Xu Y, Nagai A, Jiang D. Core-shell conjugated microporous polymers: A new strategy for exploring color-tunable and -controllable light emissions. Chem Commun, 2013, 49: 1591–1593

23 Dalapati S, Jin E, Addicoat M, *et al.* Highly emissive covalent organic frameworks. J Am Chem Soc, 2016, 138: 5797–5800

24 Dalapati S, Gu C, Jiang D. Luminescent porous polymers based on aggregation-induced mechanism: Design, synthesis and functions. Small, 2016, 12: 6513–6527

25 Bhunia A, Esquivel D, Dey S, *et al.* A photoluminescent covalent triazine framework: CO_2 adsorption, light-driven hydrogen evolution and sensing of nitroaromatics. J Mater Chem A, 2016, 4: 13450–13457

26 Wang X, Zhang C, Zhao Y, *et al.* Synthetic control and multifunctional properties of fluorescent covalent triazine-based frameworks. Macromol Rapid Commun, 2016, 37: 323–329

27 Dreyer DR, Park S, Bielawski CW, *et al.* The chemistry of graphene oxide. Chem Soc Rev, 2010, 39: 228–240

28 Huang X, Zeng Z, Zhang H. Metal dichalcogenide nanosheets: Preparation, properties and applications. Chem Soc Rev, 2013, 42: 1934–1946

29 Pakdel A, Bando Y, Golberg D. Nano boron nitride flatland. Chem Soc Rev, 2014, 43: 934–959

30 Ida S, Ishihara T. Recent progress in two-dimensional oxide photocatalysts for water splitting. J Phys Chem Lett, 2014, 5: 2533–2542

31 Das G, Biswal BP, Kandambeth S, *et al.* Chemical sensing in two dimensional porous covalent organic nanosheets. Chem Sci, 2015, 6: 3931–3939

32 Wang L, Wan Y, Ding Y, *et al.* Conjugated microporous polymer nanosheets for overall water splitting using visible light. Adv Mater, 2017, 29: 1702428

33 Wang S, Zhang C, Shu Y, *et al.* Layered microporous polymers by solvent knitting method. Sci Adv, 2017, 3: e1602610

34 Liu J, Zan W, Li K, *et al.* Solution synthesis of semiconducting two-dimensional polymer *via* trimerization of carbonitrile. J Am Chem Soc, 2017, 139: 11666–11669

35 Wang K, Yang LM, Wang X, *et al.* Covalent triazine frameworks *via* a low-temperature polycondensation approach. Angew Chem Int Ed, 2017, 56: 14149–14153

36 Jin E, Li J, Geng K, *et al.* Designed synthesis of stable light-emitting two-dimensional sp^2 carbon-conjugated covalent organic frameworks. Nat Commun, 2018, 9: 4143

37 Stegbauer L, Zech S, Savasci G, *et al.* Tailor-made photoconductive pyrene-based covalent organic frameworks for visible-light driven hydrogen generation. Adv Energy Mater, 2018, 8: 1703278

38 Xu Y, Mao N, Zhang C, *et al.* Rational design of donor-π-acceptor conjugated microporous polymers for photocatalytic hydrogen production. Appl Catal B-Environ, 2018, 228: 1–9

39 Ding H, Li J, Xie G, *et al.* An AIEgen-based 3D covalent organic framework for white light-emitting diodes. Nat Commun, 2018, 9: 5234

40 Rabbani MG, Sekizkardes AK, El-Kadri OM, *et al.* Pyrene-directed growth of nanoporous benzimidazole-linked nanofibers and their application to selective CO$_2$ capture and separation. J Mater Chem, 2012, 22: 25409

41 Luo W, Zhu Y, Zhang J, *et al.* A dynamic covalent imine gel as a luminescent sensor. Chem Commun, 2014, 50: 11942–11945

42 Kishi K, Ikeda S. X-ray photoelectron spectroscopic study of the reaction of evaporated metal films with chlorine gas. J Phys Chem, 1974, 78: 107–112

43 Yuan WZ, Zhao H, Shen XY, *et al.* Luminogenic polyacetylenes and conjugated polyelectrolytes: Synthesis, hybridization with carbon nanotubes, aggregation-induced emission, superamplification in emission quenching by explosives, and fluorescent assay for protein quantitation. Macromolecules, 2009, 42: 9400–9411

44 Hong Y, Lam JWY, Tang BZ. Aggregation-induced emission. Chem Soc Rev, 2011, 40: 5361–5388

45 Dalapati S, Jin S, Gao J, *et al.* An azine-linked covalent organic framework. J Am Chem Soc, 2013, 135: 17310–17313

46 Lin G, Ding H, Yuan D, *et al.* A pyrene-based, fluorescent three-dimensional covalent organic framework. J Am Chem Soc, 2016, 138: 3302–3305

47 Shanmugaraju S, Mukherjee PS. π-Electron rich small molecule sensors for the recognition of nitroaromatics. Chem Commun, 2015, 51: 16014–16032

48 Mallick A, Garai B, Addicoat MA, *et al.* Solid state organic amine detection in a photochromic porous metal organic framework. Chem Sci, 2015, 6: 1420–1425

49 Wei W, Lu R, Tang S, *et al.* Highly cross-linked fluorescent poly (cyclotriphosphazene-co-curcumin) microspheres for the selective detection of picric acid in solution phase. J Mater Chem A, 2015, 3: 4604–4611

50 Jun YS, Lee EZ, Wang X, *et al.* From melamine-cyanuric acid supramolecular aggregates to carbon nitride hollow spheres. Adv Funct Mater, 2013, 23: 3661–3667

51 Meng N, Ren J, Liu Y, *et al.* Engineering oxygen-containing and amino groups into two-dimensional atomically-thin porous polymeric carbon nitrogen for enhanced photocatalytic hydrogen production. Energy Environ Sci, 2018, 11: 566–571

52 Xiao J-, Shang Q, Xiong Y, *et al.* Boosting photocatalytic hydrogen production of a metal-organic framework decorated with platinum nanoparticles: The platinum location matters. Angew Chem Int Ed, 2016, 55: 9389–9393

53 Vyas VS, Haase F, Stegbauer L, *et al.* A tunable azine covalent organic framework platform for visible light-induced hydrogen generation. Nat Commun, 2015, 6: 8508

54 Zhong H, Hong Z, Yang C, *et al.* A covalent triazine-based framework consisting of donor-acceptor dyads for visible-light-driven photocatalytic CO$_2$ reduction. ChemSusChem, 2019, 12: 4493–4499

55 Fu Z, Wang X, Gardner AM, *et al.* A stable covalent organic framework for photocatalytic carbon dioxide reduction. Chem Sci, 2020, 11: 543–550

Author contributions Cheng G and Wang K designed the experiments and synthesized the materials; Cheng G performed the chemical sensor experiments and the data analyses. Wang S conducted the experiment of photocatalytic CO$_2$ reduction; Guo L and Wang Z performed the experiments of photocatalytic hydrogen evolution; Jiang J and Tan B contributed to the data analyses and discussion. Jin S conceived the project. Jin S and Cheng G co-wrote the manuscript.

Conflict of interest The authors declare that they have no conflict of interest.

Supplementary information Supporting data are available in the online version of the paper.

Guang Cheng is a PhD student at the School of Chemistry and Chemical Engineering, Huazhong University of Science and Technology, China. His research focuses on the preparation of porous organic polymers and their applications.

Shangbin Jin is an associate professor at the School of Chemistry and Chemical Engineering, Huazhong University of Science and Technology, China. He received his PhD degree from the Institute for Molecular Science, the National Institutes of Natural Sciences, Japan, and afterward conducted his postdoc research at the National Institute for Materials Science, Japan. His current research interests mainly focus on the synthesis of covalent triazine frameworks and their photofunctional applications.

面向高性能传感和光催化应用的芘基共价三嗪框架

程光[1†], 王科伟[2†], 汪圣尧[4†], 郭莉萍[1], 王梓鉴[3], 蒋加兴[3], 谭必恩[1], 金尚彬[1*]

摘要 多孔有机聚合物(POPs)是一类新兴的多孔材料, 在多个领域有着广阔的应用前景. 其中, 具有共轭多孔结构的共价三嗪框架(CTFs)在光电子学中具有良好的应用前景. 为了获得高性能的光电材料, 通常基于合适的构建单元设计是构建CTFs至关重要的途径. 本文报道了两种基于典型荧光构建单元的新型荧光CTF的合成, 其中CTF-Py是首次由芘(Py)构建单元构建而成, 在高灵敏度硝基芳烃传感中显示了一定的应用前景, 并在光催化水分解和二氧化碳还原中展现了良好的催化性能.